






ARTICLE

<https://doi.org/10.1038/s42003-019-0733-7>

OPEN

Collective exchange processes reveal an active site proton cage in bacteriorhodopsin

Daniel Friedrich ^{1,2,5,6}, Florian N. Brüning ³, Andrew J. Nieuwkoop ^{1,7}, Roland R. Netz ³, Peter Hegemann ⁴ & Hartmut Oschkinat^{1,2*}

Proton translocation across membranes is vital to all kingdoms of life. Mechanistically, it relies on characteristic proton flows and modifications of hydrogen bonding patterns, termed protonation dynamics, which can be directly observed by fast magic angle spinning (MAS) NMR. Here, we demonstrate that reversible proton displacement in the active site of bacteriorhodopsin already takes place in its equilibrated dark-state, providing new information on the underlying hydrogen exchange processes. In particular, MAS NMR reveals proton exchange at D85 and the retinal Schiff base, suggesting a tautomeric equilibrium and thus partial ionization of D85. We provide evidence for a proton cage and detect a preformed proton path between D85 and the proton shuttle R82. The protons at D96 and D85 exchange with water, in line with *ab initio* molecular dynamics simulations. We propose that retinal isomerization makes the observed proton exchange processes irreversible and delivers a proton towards the extracellular release site.

¹ Leibniz-Forschungsinstitut für Molekulare Pharmakologie, Robert-Rössle-Str. 10, 13125 Berlin, Germany. ² Freie Universität Berlin, Institut für Chemie und Biochemie, 14195 Berlin, Germany. ³ Freie Universität Berlin, Fachbereich Physik, 14195 Berlin, Germany. ⁴ Humboldt-Universität zu Berlin, Institut für Biologie, Invalidenstr. 42, 10115 Berlin, Germany. ⁵ Present address: Department of Molecular and Cellular Biology, Harvard University, 52 Oxford Street, Cambridge, MA 02138, USA. ⁶ Present address: Department of Cancer Biology, Dana-Farber Cancer Institute, 360 Longwood Avenue, Boston, MA 02215, USA. ⁷ Present address: Department of Chemistry and Chemical Biology, Rutgers, The State University of New Jersey, 123 Bevier Road, Piscataway, NJ 08854, USA.

*email: oschkinat@fmp-berlin.de

Bacteriorhodopsin (BR) is an excellent model system to establish new approaches for studying protonation dynamics^{1–4}; signals of exchanging protons may be observed in the protein interior for entropic reasons due to their tight coordination within hydrogen bonding networks and limited exchange with bulk water (Fig. 1a, b)^{5–7}. The BR pore features three sites with distinct protonation dynamics characteristics, intensely discussed in the literature⁴: the uptake site (D96 and H₂O 502), the active site (D85, D212, R82, retinal Schiff base (RSB), and H₂O 401, 402, and 406), and the proton release group (E194, E204 and a trimeric water cluster (H₂O 403, 404, and 405)) (Fig. 1a). According to the current understanding of the photocycle⁸, BR relocates in non-consecutive transport steps a proton across the membrane out of the *Halobacterium salinarum* cell (Fig. 1c)^{9–12}. Light reception by the BR₅₆₈ dark-state results in the excited electronic state S1, with the retinal chromophore isomerizing from an all-*trans*,15-*anti* to a 13-*cis*,15-*anti* configuration during the transition to K₅₉₀. In this K₅₉₀ intermediate, however, the chromophore is not fully isomerized yet¹³. The reaction completion requires a subsequent relaxation of retinal into the 13-*cis*,15-*syn* configuration (L₅₅₀ state). This is caused by a drastic pK_a drop of the RSB and an increase of the D85 pK_a accompanied by a proton transition from the RSB to D85, leading to an absorption blue shift to 412 nm (M1₄₁₂)¹⁴. Protonation of D85 initiates an outward movement of R82 (towards the extracellular site of the protein), a decrease in pK_a of the proton release group and a proton release into the extracellular bulk phase (L₅₅₀ → M1₄₁₂)^{14–17}. After reorientation of Helix F and large structural changes (M1₄₁₂ → M2₄₁₂), water is invading into the proton channel and the RSB is reprotonated from D96 via a transient water chain in the M2₄₁₂ → N₅₂₀ transition¹⁸. Subsequently, protonation of the RSB reduces the pK_a of D85 causing a proton transfer from D85 to the proton release group (N₅₂₀ → O₆₄₀). To bridge the long distance between these two sites, this proton relocation step requires additional sites for proton transport, e.g., H₂O molecules or the R82 guanidinium group (Fig. 1a, b). However, it remained unclear whether this late proton transfer involves deprotonation and reprotonation of R82¹⁹. The photocycle is then completed by restoring the initial all-*trans* configuration of the retinal by thermal relaxation (O₆₄₀ → BR₅₆₈)²⁰. Key steps in this proton transport process involve H₂O molecules^{4,21}. This is especially true for the proton movement from D96 to the RSB but also for

the proton release from D85 towards the proton release group (Fig. 1a, b).

Recently, time-resolved studies using serial femtosecond crystallography revealed structural dynamics of retinal isomerization and repositioning of water molecules during the BR photocycle in the active site^{2,3}. These studies showed moderate structural changes at the beginning of the photocycle before retinal isomerization, not considering proton relocation independent of heavy atom movements. However, knowledge of preformed proton communication pathways between key sites (e.g., RSB, D85, R82, and the proton release group, the former three forming the active site proton cage) is essential for understanding BR function. Such protonation dynamics within the hydrogen bonding network may involve, for example, proton oscillations at the RSB and D85 as well as hydroxide and hydronium ions in place of proximate water molecules already in the dark-state, which may be indicated by proton nuclear magnetic resonance (NMR) signals with their characteristic chemical shifts. We analyzed the underlying chemical exchange processes site-specifically by magic angle spinning (MAS) NMR and in particular exchange spectroscopy²². In this context, the role of R82 in the proton transport mechanism and the nature of water 402 are elucidated in detail because time-resolved infrared spectroscopy for these sites is not available. To this end, we studied deuterated and ¹³C,¹⁵N-labeled native BR-enriched membranes (purple membranes). Direct proton detection was employed in a temperature range from 100 K to 290 K to monitor protons in the BR dark-adapted state (mixture of 13-*cis*,15-*syn* and 13-*trans*,15-*anti* retinal configurations) at key sites of the proton transport pathway, after introducing a subset of exchanging protons into the interior of the perdeuterated samples upon illumination. It is well-established that the structural rearrangements during the photocycle are required for complete proton transport through the BR pore from the uptake to the release site, which is exploited here for reprotonation of sites involved in the pathway^{9,23–25}. Proton-detected MAS NMR exchange spectroscopy enabled the observation of proton localization and displacement, and the underlying exchange. It informs on exchange contributions of the chemical sites involved in the global proton relocation process of BR, even when investigating the dark-adapted equilibrium that potentially features different proton exchange rates compared to the transfer steps during the photocycle. Ab initio molecular dynamics simulations allowed for an estimation of proton

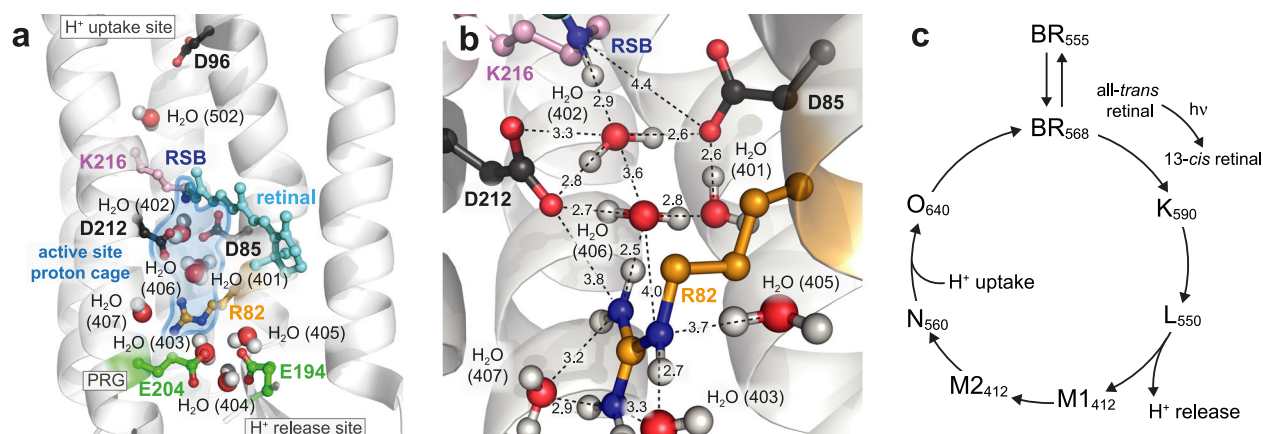


Fig. 1 The light-driven proton pump bacteriorhodopsin (BR, pdb 1c3w). **a** The proton transport pathway of BR involves D96 at the proton uptake site, D85, the retinal Schiff base (RSB) that is covalently bound to K216, and R82 in an active site proton cage. The extracellular proton release site is composed of the proton release group (PRG) with two glutamic acids (E194 and E204) and three water molecules. **b** The active site proton cage includes the RSB, D85, R82, and the H₂O molecules 401, 402, and 406. Dashed lines indicate distances in Å. **c** The photocycle of BR. The numbers correspond to the maximum absorption wavelength of the respective intermediate.

distribution between a H₂O molecule and two carboxyl groups, a simplified model for proton displacement in the D85 environment.

Results

Resonance assignments of exchangeable protons in BR. As a first step, we monitored the efficiency of proton back-exchange by recording a proton-detected, two-dimensional ¹⁵N–¹H correlation using cross polarization-based magnetization transfers exploiting dipolar, through-space couplings on light-exposed purple membranes with fast MAS (Supplementary Fig. 1)^{26,27}. The spectrum indicates significant back-exchange of approximately 70 amino acids as shown by the respective backbone amide signals, corresponding to 28% of the residues. Based on a set of triple-resonance experiments²⁸, we could assign approximately 59% of these signals (Supplementary Figs. 1, 2 and Supplementary Table 1), reflecting indeed amide groups of residues in loops or in solvent accessible areas as is often seen in MAS NMR studies of deuterated membrane proteins (Supplementary Fig. 3)²⁹. The well-dispersed amide group signals with a chemical shift pattern characteristic for α -helices clearly suggest that BR adopts its native seven-transmembrane helix fold (Supplementary Fig. 1). The ¹⁵N–¹H correlation and the observed ¹³C α and ¹³C β chemical shifts agree well with previous NMR studies of purple membranes^{30,31}. However, none of these assigned backbone resonances correspond to residues involved in proton pumping; we therefore applied the following strategy to study sites that contribute to proton displacements during BR molecular action.

Protons in the proximity to the carboxyl groups of D96, D85, at the guanidinium group of R82, and involving nearby H₂O molecules were probed by a combination of two-dimensional ¹⁵N–¹H (Fig. 2a, b), ¹³C–¹H (Fig. 2a, c), both cross polarization-based, and ¹H–¹H exchange spectroscopy (Fig. 2a, d) of BR wildtype purple membranes. We further investigated in this way BR mutated at the proton donor of the RSB (D96), the acceptor of the RSB proton (D85) and the proton shuttle R82: D96N, in which the reprotonation of the RSB is dramatically slowed down³², D85T that features a red-shift of the BR-absorption and complete inactivation of proton pumping^{33,34}, and R82Q, in which BR-absorption is red-shifted, the RSB-pK_a lowered, and proton shuttling from D85 to the proton release group severely hampered^{35,36}.

Comparison of the ¹³C–¹H correlations of wildtype purple membrane and of the mutant D96N yields the C γ chemical shift of D96, in accordance with earlier assignments by the Engelhard group³⁷, and the shift of the attached proton (Fig. 2c and Supplementary Table 2). The ¹H–¹H exchange spectrum of D96N confirms the assignment of the signal at 11.0 ppm ¹H chemical shift to D96–H δ^2 (Fig. 2d and Supplementary Fig. 4). In the BR wildtype spectrum, the carboxylic acid proton of D96 shows a cross peak at the water frequency due to chemical exchange with H₂O (Fig. 2a, d). Employing the cross polarization-based ¹³C–¹H spectrum of the D85T mutant (Fig. 2c), the signal at 12.1 ppm ¹H chemical shift in the wildtype spectra can be formally assigned to D85–H δ^2 (Fig. 2a, c, d and Supplementary Table 2). The observed D85–C γ resonance agrees well with the assignment obtained in earlier studies³⁷. This is also confirmed by the missing diagonal and cross peaks at the D85–H δ^2 frequency in the ¹H–¹H exchange spectrum of D85T, even when taking different signal-to-noise ratios into consideration (Fig. 2d and Supplementary Fig. 4). The Hⁿ of R82 can be assigned to a signal at 6.2 ppm ¹H chemical shift as it disappears in the ¹⁵N–¹H spectrum of the BR mutant R82Q (Fig. 2b and Supplementary Table 2).

Proton exchange detected at room temperature by MAS NMR.

The observed proton signals, including their cross peaks in the exchange spectra are intriguing. In general, the presented exchange spectra include contributions from chemical and spin exchange, however, we assume the latter to be of minor importance due to the distances between the diluted protons investigated and the high MAS frequencies applied, which significantly reduce spin diffusion based on dipolar couplings. The signal at 12.1 ppm is assigned to be in the vicinity of the D85 side chain carboxyl group and may reflect either protonation of D85 or a hydronium ion (occurring typically at 12–14 ppm³⁸), or the chemical shift average of both. Formally, several tautomeric states are possible for the cluster involving the RSB, water 402, and D85 (Fig. 2e). For water 402 that is close to the carboxyl group of D85 (Fig. 1b), proton displacement can lead to partially populated hydroxide and hydronium ion states as well as to a protonated D85 form (Fig. 2e). The hydroxide ion occurs in conjunction with a D85 carboxyl group proton, and the hydronium ion requires D85 to be non-protonated (Fig. 2e). D85 should therefore be considered as partially ionized under the applied experimental conditions. We will refer to the respective proton signal as D85–H δ^2 . To analyze this situation further, cross polarization build-up experiments were additionally recorded for the D85 and D96 C γ –H δ^2 cross peaks (Supplementary Fig. 5). The D96 signal builds up faster than the D85 peak, indicating that the carboxylic acid proton in the D85 case is, on average, more distant from the C γ and therefore closer to H₂O in comparison to D96. However, varying D85 and D96 side chain mobilities represent an additional source for the observed differences in cross polarization build-up. Similar to D96–H δ^2 , D85–H δ^2 exhibits a cross peak to H₂O in the BR wildtype exchange spectrum (Fig. 2a, d). In contrast to D96–H δ^2 , the exchange peak of D85–H δ^2 at the water frequency has a much higher intensity as the corresponding diagonal peak. Intensities of diagonal peaks in exchange spectra are directly correlated to the populations, whereas those of cross peaks are additionally modulated by the kinetics of the exchange process between the two nuclei giving rise to the cross peak as well as by the populations of their respective states. In line with the above-mentioned cross polarization build-up experiments (Supplementary Fig. 5), the observed intensity differences therefore suggest that the localization of D85–H δ^2 is in favor of the chemical environment of water, which could explain that it was not observed by vibrational spectroscopy so far. Collectively, our data provide evidence that D85–H δ^2 is exchanged within the hydrogen bond between D85 and one of the H₂O molecules close to it (Figs. 1b, 2a, c–e and Supplementary Figs. 4 and 5).

The BR wildtype exchange spectrum shows a cross peak between R82 and D85–H δ^2 at 6.2 and 12.1 ppm ¹H chemical shift, respectively, which may reflect a signal due to long-range proton exchange between the carboxyl group of D85 and the guanidinium group of R82, potentially via the structurally close water molecules 401 and 406 (Figs. 1b, 2a, d and Supplementary Fig. 4)⁵. In general, we cannot distinguish different water populations spectroscopically, including bulk water and protein-bound water molecules. Thus, proton exchange between amino acids and the sum of all water molecules is observed. This may be resolved if smaller ¹H linewidths could be achieved by even higher MAS frequencies, or through ¹⁷O spectroscopy at very high magnetic fields. As expected, the R82–Hⁿ signal is missing in the ¹H–¹H exchange spectra of the R82Q and D85T mutants, since R82–Hⁿ is indirectly observed via D85–H δ^2 detection in the wildtype (Fig. 2a, d and Supplementary Fig. 4). For BR wildtype, these findings show that there is a proton translocation pathway to the R82 guanidinium group and, consequently, R82 should be considered as an intermediate in proton relocation serving as an

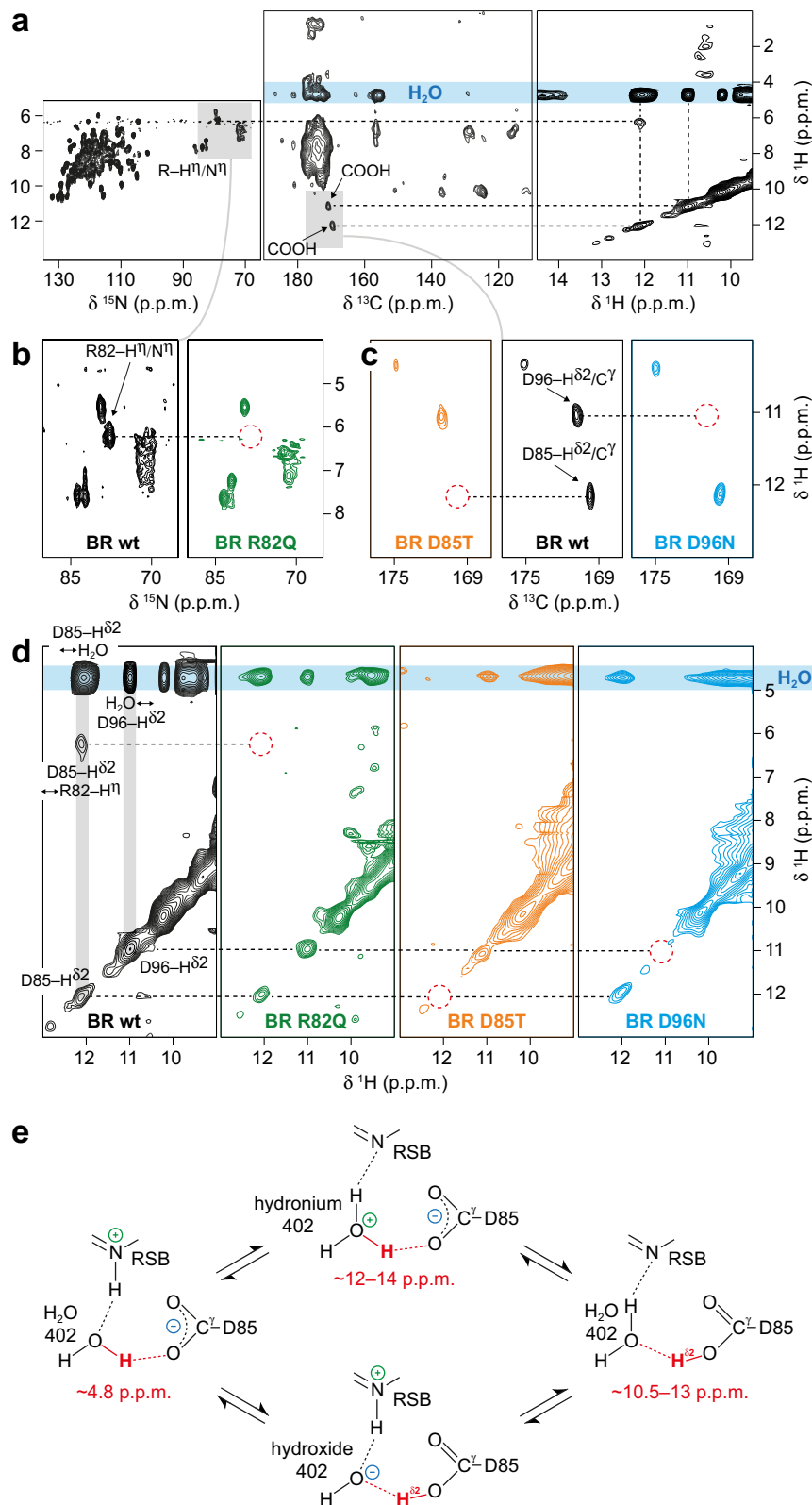


Fig. 2 Protonation states and chemical exchange of protons at R82, D96, D85, and water molecules in bacteriorhodopsin (BR) probed by proton-detected MAS NMR at room temperature. **a** ^{15}N - ^1H (left), ^{13}C - ^1H (middle), and ^1H - ^1H exchange (right) spectra of BR wildtype. **b** ^{15}N - ^1H correlations of BR wildtype (wt, black spectrum) and the mutant R82Q (green spectrum). **c** ^{13}C - ^1H correlations of BR wildtype (wt, black spectrum) and the D85T and D96N mutants (orange and blue spectra, respectively). The mutants are used to assign the signals of D96- $\text{H}^{\delta 2}$ (11.0 ppm), D85- $\text{H}^{\delta 2}$ (12.1 ppm) and R82- H^η (6.2 ppm). Red dashed circles indicate missing signals resulting from mutations that allow the assignment. **d** ^1H - ^1H exchange spectra of BR wildtype (wt, black spectrum), R82Q (green spectrum), D85T (orange spectrum) and D96N (blue spectrum). **e** At H₂O 402, both hydronium and hydroxide ions are possible, affecting the proton localization through exchange within the hydrogen bonds to the retinal Schiff base (RSB) and D85. The observed chemical shifts for the proton highlighted in red agree with tautomeric structures involving H₂O 402, a hydronium 402 and a carboxyl group proton at D85.

active proton donor and acceptor on the way from D85 towards the proton release group.

In summary, an exchange signal is observed between D85 and R82, indicating a proton pathway between these two residues. In addition, both the D85 and D96 carboxyl groups show chemical exchange of protons with H₂O in the BR dark-state upon illumination as seen after ¹H/²H back-exchange. Illumination allowed protons to enter the pore of BR via exchangeable sites involved in the proton transport pathway. We conclude that in both cases, D85 and D96, a proton undergoes displacement between the carboxyl group and H₂O. The exchange between D85 and H₂O may lead to a hydronium ion state at H₂O 402.

RSB proton exchange observed by MAS NMR at variable temperatures. In agreement with the occurrence of a dynamic process (Fig. 2e), we see exchange broadening of the RSB proton or nitrogen signal (Fig. 3a), indicating that the so far observed exchange in the active site proton cage involves the RSB NH moiety as well (Figs. 1b, 2e). In a previous study, the RSB nitrogen signal could be observed at around 100 K in the spectral region of 165–175 ppm for the BR dark-state¹⁰. In a similar, recent experimental approach involving measurements at around 100 K, the signal of the RSB proton itself could be detected at 13.2 and 12.2 ppm for BR₅₅₅ (13-*cis*,15-*syn* retinal configuration) and BR₅₆₈ (13-*trans*,15-*anti* retinal configuration), respectively³⁹. At room temperature, such proton resonances are not observed. To examine the situation further, we performed proton-detected MAS NMR measurements between 97 and 273 K (Fig. 3a). At temperatures below 200 K, we observe well-resolved signals of the RSB NH moiety at 13.2 ppm (BR₅₅₅, ¹⁵N chemical shift of 173.5 ppm) and 12.2 ppm ¹H chemical shift (BR₅₆₈, ¹⁵N chemical shift of 165.4 ppm) in agreement with the previous studies (Fig. 3a and Supplementary Table 2)^{10,39}. Above 200 K, however, the signal-to-noise ratios of the two RSB proton resonances decrease and both signals vanish towards 273 K, where they are not observable anymore (Fig. 3a, red spectrum in the very right panel, bottom). In general, multiple factors such as temperature-induced changes in cross polarization efficiency and Boltzmann distribution can lead to different sensitivity in these experiments. To compensate for this, we recorded the spectra with optimized cross polarization transfers and similar measurement time by adjusting the number of scans, and taking into account that $T_1(^1\text{H})$ changes with temperature, applying different recycle delays (in each experiment set to $1.3 \times T_1(^1\text{H})$). Another possible explanation for the disappearance of the two RSB proton signals could be conformational exchange between the 13-*cis*,15-*syn* and 13-*trans*,15-*anti* retinal configurations in the $\mu\text{s}/\text{ms}$ time regime. If this would be the case, however, it would not take 21 min to reach equilibrium of the 40/60% distribution of these isomers as measured by Oesterhelt et al.⁴⁰. The low B-factors of the active site⁵, including the RSB, in the crystal structure and the well-defined, sharp NMR signals observed at low temperature further indicate high structural homogeneity. This excludes other conformational dynamics in the protein that could potentially lead to the observed line broadening, in agreement with previous studies employing molecular dynamics simulations by the Elstner group⁴¹. We thus conclude that the RSB proton signal loss is attributed predominantly to line broadening caused by chemical shift exchange. Such an effect can result from proton exchange leading to disappearance of signals in NMR spectra due to coalescence. Therefore, these data suggest that the RSB proton is displaced at room temperature, involving exchange with H₂O 402 (Figs. 1b, 2e). Remarkably, the ¹H chemical shifts of 12.2 and 13.2 ppm for the RSB proton agree again well with a signal expected for a hydronium ion, similar to the situation of D85 (Fig. 2e). This

exchange may thus be coupled to the observed proton displacement between D85 and H₂O 402, causing potential collective proton exchanges within the hydrogen bonding networks (Fig. 2e). Even though a high proton affinity of the RSB has been measured by bulk phase pH titration⁴², so far no evidence exists for a proton path to the exterior of the protein in the dark-state and the reported pK_a of 13.3 must be therefore considered as apparent, still enabling proton oscillation at the RSB and water 402. After long discussions in the literature, it has been accepted that D85 and D212 are the only deprotonated aspartates in darkness^{32,43,44}. However, our findings suggest that D85 is exchanging rapidly a proton with H₂O 402 and/or 401 even in the dark, presumably eased by or coupled to proton displacement between the RSB and H₂O 402.

Characterization of proton exchange between carboxyl groups and H₂O. To provide a model for proton displacement in a protein environment, we performed ab initio molecular dynamics simulations to compute the proton distribution in a simplified configuration, consisting of an H₂O molecule located between two carboxyl groups with one excess proton, i.e., the system has a net charge of 1 e⁻ (Fig. 3b, see Methods section for details). This model mimics the water molecule 402 that is coordinated by D212 and D85 (Fig. 1b) and thus enables an analysis of primary, thermally activated proton oscillations in the BR active site. The distances between the two carboxyl groups, and the positions of the central water molecule and of the protons are not fixed but are subject to thermal fluctuations. Depending on the distance between the carboxylic acid and water oxygens ($r_{\text{O}_c\text{O}_w}$), the relative position of proton 2, described by an asymmetry coordinate ($r_{\text{O}_c\text{H}-\text{O}_w\text{H}}$, Fig. 3b), exhibits different behavior⁴⁵. Note that a negative asymmetry refers to the proton localized near the carboxyl group oxygen, and a positive asymmetry near the water oxygen. For $r_{\text{O}_c\text{O}_w}$ of 2.4–2.6 Å, intermediate positions of proton 2 are frequently observed, while for large values of $r_{\text{O}_c\text{O}_w}$ the proton tends to be localized near the central water molecule, as can be seen from the free energy distribution in Fig. 3c. This means that dynamic proton exchange is observed in time-resolved trajectories, from which a mean residence time of about 1 ps is determined (Fig. 3d). The analysis of the typical distances between the protons and oxygen atoms reveals that bifurcated, three-centered hydrogen bonds⁴⁶ do not appear in the model system (Supplementary Fig. 6). The proton transfer from the water oxygen to a carboxyl group involves a free-energetic barrier of about $3 k_B T$ as a function of the asymmetry reaction coordinate $r_{\text{O}_c\text{H}-\text{O}_w\text{H}}$, as shown in Fig. 3e. In fact, Eckert and Zundel found a $6 k_B T$ barrier for a fixed $r_{\text{O}_c\text{O}_w}$ of 2.65 Å from static ab initio self-consistent field calculations⁴⁷. It is not surprising that the barrier height is smaller in our dynamic simulation which allows for kinetic relaxation of all positions. In BR, $r_{\text{O}_c\text{O}_w}$ is 2.6 Å between D85 and the well-defined H₂O 402 that shows low B-factors in the crystal structure solved at cryogenic temperatures (100 K) (Fig. 1b)⁵. However, the NMR experiments were performed at around 290 K, therefore a slightly shorter distance $r_{\text{O}_c\text{O}_w}$ for D85 and H₂O 402 is possible as well. Such variation in distances agrees well with molecular dynamics simulations of the Gerwert group⁴⁸, and has been observed by time-resolved serial femtosecond crystallography at room temperature^{2,3}. In our experiments, a proton undergoing similar displacement gives rise to an NMR signal at 12.1 ppm, reflecting the chemical shift of D85-H^{δ2} or its time-weighted average with the proton chemical shift of a hydronium ion (12–14 ppm) (Fig. 2a, c–e and Supplementary Figs. 4 and 5). Worth of note, both H₂O 401 and 402 have the same distance of 2.6 Å to D85-O^{δ2} and form a pentameric hydrogen bond arrangement together with D85, D212, and H₂O 406 (Fig. 1b)^{4,5}.

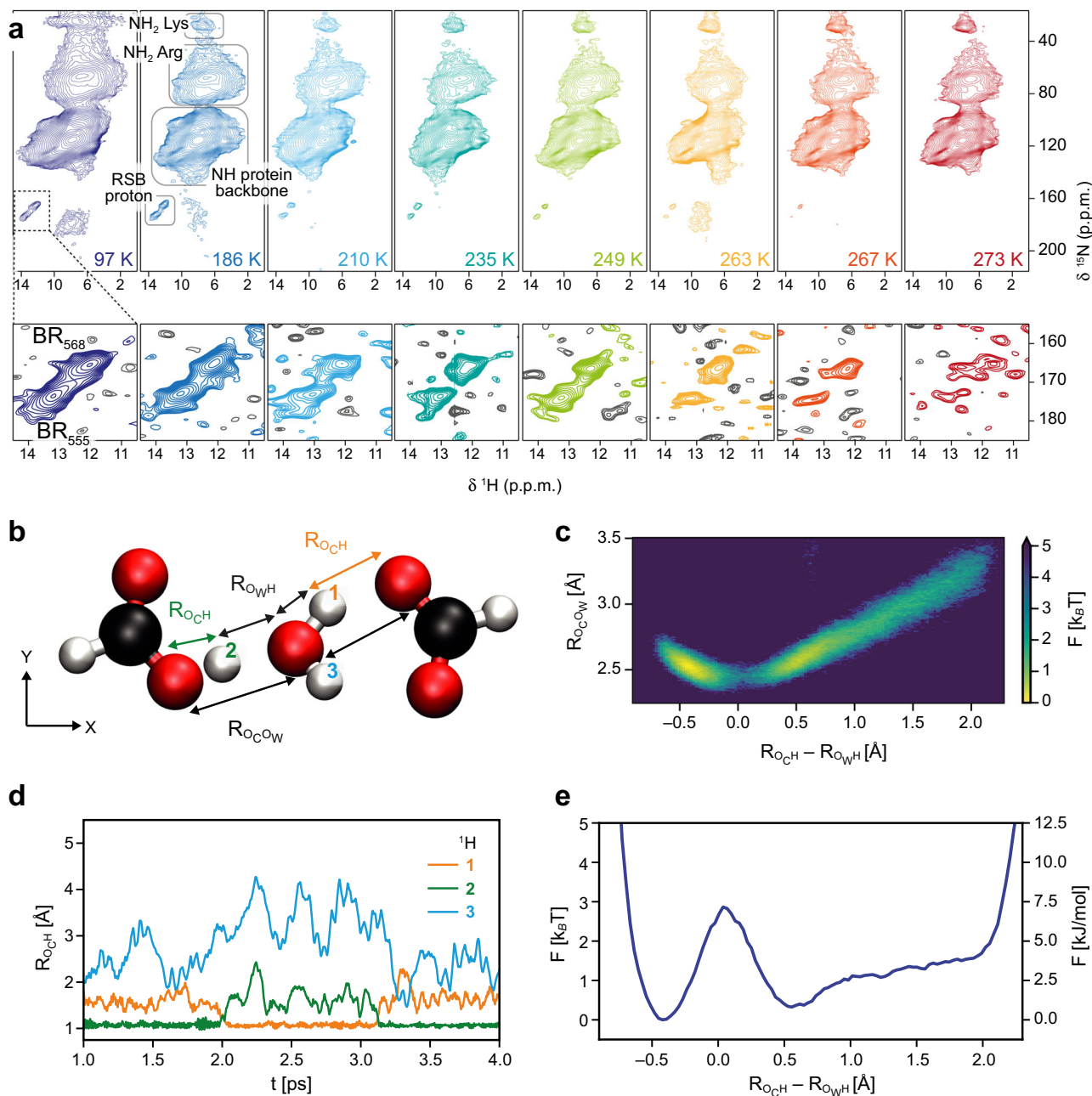


Fig. 3 Observation of retinal Schiff base (RSB) proton dynamics by MAS NMR and characterization of proton exchange by *ab initio* molecular dynamics simulations in a model system. **a** Proton-detected, two-dimensional ^{15}N - ^1H correlation spectra of purple membrane in bacteriorhodopsin (BR) dark-state recorded at temperatures ranging from 97 K (dark blue spectrum) to 273 K (red spectrum). The spectral region of the RSB proton signals for BR₅₆₈ and BR₅₅₅ is plotted at the noise level (bottom panels, positive contours are color-coded according to the temperature and negative contours are shown in gray). **b** The proton distribution is analyzed by *ab initio* molecular dynamics simulations in a model system consisting of one H₂O molecule, two carboxyl groups and one excess proton which are all subject to thermal positional fluctuations. The distance between carboxyl group and water oxygen atoms ($R_{\text{O}^-\text{O}_\text{W}}$) and the excess proton's relative asymmetry with respect to the two oxygens ($R_{\text{O}^-\text{H}} - R_{\text{O}_\text{W}\text{H}}$) are used as effective reaction coordinates. **c** The free energy landscape of the proton is shown as a function of the coordinates, as defined in **b**. **d** Trajectories of the distances, $R_{\text{O}^-\text{H}}$, of the three central hydrogens labeled as in **b** to the respective closest carboxyl group oxygen. The proton exchange is well visible as a fast jump process: proton 1 resides near the closest carboxyl group oxygen for about 1 ps in the time interval from $t = 2.0$ ps to $t = 3.1$ ps. **e** The free energy of the protons projected onto the asymmetry coordinate ($R_{\text{O}^-\text{H}} - R_{\text{O}_\text{W}\text{H}}$) indicates a low proton transfer barrier of about $3 k_{\text{B}}T$.

Discussion

In the present study, we characterize protonation dynamics in the BR dark-adapted state, revealing a proton cage close to the Schiff base and displacement of protons at D85 and H₂O 402. The proton cage extends to R82 which is involved in a hydrogen bonding network with water molecules and the carboxyl group of D85 (Fig. 1b)⁴⁵. R82 acts as a regulator of the D85 pK_{a} , but a

transient deprotonation of it has neither been unequivocally observed nor excluded^{19,49,50}. The detected protonated form of R82 and the exchange signal correlating R82-H¹ and D85-H^{δ2} suggest chemical exchange between both residues within this network, presumably via the water molecules 401 and 406 as these, based on the dark-state crystal structure solved at 100 K, may provide a direct connection via a hydrogen bond network

(Figs. 1b, 2a, b, d)⁵. This reveals a proton path between D85 and R82, highlighting the involvement of the R82 guanidinium group in proton pumping. The observed proton exchange between the RSB, water molecules, D85 and R82 indicate the existence of a pathway across the proton cage at the BR active site (Figs. 1a, b, 2, 3a). After retinal isomerization upon light reception, the underlying exchange equilibrium involving R82 and D85 might be shifted towards the protonated form of D85 during the L₅₅₀ → M₁₄₁₂ transition. Potentially, this change in equilibrium is facilitated by the structural changes detected by time-resolved serial femtosecond crystallography^{2,3}. The MAS NMR exchange spectra show exchange of R82–H^{δ2} already in the dark-state which supports the possibility of R82 deprotonation in the L₅₅₀ → M₁₄₁₂ transition (Figs. 1b, c, 2a, d).

The detected protonation of D96 in the BR dark-state agrees well with previously obtained Fourier-transform infrared spectroscopy results⁴. D96 serves as the central binding position in the proton uptake site in conjunction with H₂O molecules located at the cytoplasmic entry of the protein pore (Fig. 1a). It has been proposed that the D96–H^{δ2} is relocated via a transiently established chain of three water molecules to the RSB in a Grotthuss-type mechanism upon the M₂₄₁₂ → N₅₂₀ transition as revealed by molecular dynamics simulations (Fig. 1c)¹⁸. The observed proton exchange between D96 and water in BR₅₆₈, however, requires H₂O molecules close to the carboxyl group already in the BR dark-state. The next water molecule, H₂O 502, occurs at a distance of 5.0 Å to the D96–O^{δ2} along the proton transport pathway towards the RSB, as measured in the crystal structure solved at 100 K (Supplementary Fig. 7)⁵. We thus suggest that, in the BR dark-state, water molecule 502 may be rather dynamic at room-temperature in contrast to the situation at cryogenic temperatures. The possibility of proton displacement between D96 and water molecules at the cytoplasmic entry site of the BR pore can be largely excluded due to low water accessibility in the dark-state⁴⁸. Additional water molecules not resolved in the crystal structures represent another possible explanation for the proton exchange observed between these sites. In any case, the D96–H^{δ2} can exchange with a water molecule in the dark-adapted BR₅₆₈ state.

In conclusion, we have directly observed signals of exchangeable protons at key sites including the RSB, D96, D85, and R82 in purple membranes using proton detection by fast MAS NMR. We have further detected chemical exchange of these protons with water, in particular within the active site proton cage of dark-adapted BR₅₆₈. Our experiments point towards oscillations between intermittently occurring tautomeric structures including a hydronium ion in place of water 402 and a protonated D85 form. The ab initio molecular dynamics simulations show proton residence times of 1 ps in a model system. Displacement of the RSB proton corroborates coupling of the observed proton exchange processes between the RSB, D85, and R82 via H₂O molecules in the active site proton cage, indicating reversible proton displacement in the dark-state. Intriguingly, the distances between the RSB and D85 hydrogen bond acceptors and the oxygen of water 402 are 2.6 Å. This is slightly longer than expected for an ideal hydrogen bond. We assume this promotes the oscillation between different states, as highlighted by the ab initio molecular dynamics simulations on proton displacement between H₂O and two carboxyl groups which are reflecting the counter ion geometry. The potential involvement of R82 in proton transport is supported by an exchange signal involving the carboxyl group of D85 in dark-adapted BR. As proton pumping by BR is a directed process, we suggest that retinal isomerization makes the observed chemical exchange within the proton cage irreversible through disrupting the proton oscillation via tilting of the RSB, resulting in the extracellular release of a proton.

Methods

Preparation of ²H,¹³C,¹⁵N-labeled purple membrane. For production of purple membranes of bacteriorhodopsin, the *Halobacterium salinarum* strains BR-wild-type, BR-R82Q, BR-D85T, and BR-D96N from Janos Lanyi, Dieter Oesterhelt and Markus Lange, Actilor GmbH were used. The following procedures were the same for all four strains. Cells were grown in deuterated cel-tone medium for at least 10 days at 37 °C at 100 rpm in shaking flasks, after pre-culturing in protonated medium. In 200 mL, the sterile filtered medium contained, both in deuterated and protonated form: 1 g ¹³C,¹⁵N-cel-tone, 50 g NaCl, 0.4 g KCl, 4 g MgSO₄, 0.04 g CaCl₂, 0.6 g Na-citrate (C₆H₅Na₃O₇·7H₂O), 0.4 mg Biotin, 0.4 mg Thiamin, 0.06 μg MnSO₄, 0.72 μg FeCl₂, 0.088 μg ZnSO₄, and 0.01 μg CuSO₄ at pH 7. Cells were harvested at 7000 rpm for 20 min at 4 °C in a Beckman JLA 8.1 rotor with 1 L tubes. The supernatant was discarded and cells were resuspended in 6 mL basal salt (250 g/L NaCl, 20 g/L MgSO₄·7H₂O and 2 g/L KCl at pH 7). After adding DNase (grade II) and 65 mL H₂O, the cell suspension was dialyzed over night at 4 °C against H₂O under stirring. Membranes were then collected via centrifugation for 60 min at 40,000 rpm and 4 °C with a Sorvall 90SE ultracentrifuge using a 45Ti rotor. 3 mL of 50 mM Tris-HCl at pH 7.4 were used to resuspend the pellet, and the membranes were homogenized and fractionated by density gradient centrifugation using saccharose (30–70%) for 14 h at 22,000 rpm and 15 °C with a Sorvall 90SE ultracentrifuge using a TST-28 rotor. The purple membrane fraction was collected and concentrated for 1 h at 40,000 rpm and 4 °C with a Sorvall 90SE ultracentrifuge using a 45Ti rotor. After washing with 50 mM Tris-HCl at pH 7.4, followed by homogenization and concentrating again (this procedure was performed twice), the purple membranes were stored at –20 °C.

Sample preparation for solid-state MAS NMR measurements. The purple membranes were diluted to 0.01 OD in 90%/10% ¹H₂O/²H₂O 50 mM Tris-HCl at pH 7.4 and illuminated (a 595 nm filter was used) for 4 h under stirring in a water-cooled cuvette at 15 °C with a home-build illumination set-up. We thus assume that each bacteriorhodopsin molecule went through the photocycle during this photo-equilibration, thereby pumping protons and back-exchanging protons at key sites of the proton transport pathway (including the D85, D96, and R82 side chains, the retinal Schiff base and water molecules). The purple membranes were then collected by ultracentrifugation for 2 h at 150,000 × g and 4 °C, and packed into 1.9 mm (for 20 and 40 kHz MAS experiments) or 1.3 mm (for 60 kHz MAS experiments) Bruker MAS NMR rotors using home-made filling tools. Rotors were sealed with silicone rubber disks to avoid loss of liquid during MAS. Before starting acquisition of MAS NMR experiments, the samples were equilibrated in the dark (in the MAS NMR probe inside the magnet) for at least 1.5 h to allow for establishing the BR dark-adapted state, i.e., the mixture of the 13-*cis*,15-*syn* and 13-*trans*,15-*anti* retinal configurations, which has been measured to reach equilibrium after 21 min⁴⁰.

Solid-state MAS NMR measurements. NMR experiments were performed on Bruker Avance III spectrometers with ¹H Larmor frequencies of 800 and 900 MHz using 1.3 mm triple-resonance (HCN) and 1.9 mm four-channel (HCND) Bruker MAS probes, respectively. The variable temperature was controlled using a Bruker cooling unit and adjusted to 260 K and 230 K for 60 kHz MAS experiments with the 1.3 mm probe and 40 kHz MAS experiments with the 1.9 mm probe, respectively. According to external temperature calibration, this corresponds to actual sample temperatures of 291 K for the 1.3 mm probe and 293 K for the 1.9 mm probe. The temperature-dependent detection of RSB proton dynamics was performed at 20 kHz MAS on a 800 MHz Bruker Avance III spectrometer using a 1.9 mm four-channel dynamic nuclear polarization probe. A cross polarization-based (H)NH pulse sequence with MISSISSIPPI solvent suppression⁵¹ was applied at actual sample temperatures of 97, 186, 210, 235, 249, 263, 267, and 273 K. The temperature was adjusted with a Bruker LT/MAS unit. The ¹H–¹⁵N and ¹⁵N–¹H transfers were optimized around $w_1^H = 3\omega_R/2$ and $w_1^X = 1\omega_R/2$. For each experiment, the recycle delay was set to $1.3 \times {}^1H(T_1)$ as measured via inversion recovery. The number of scans was adjusted such that each experiment had the same measurement time of about 16 h with identical acquisition times and spectral windows.

The ¹H–¹H exchange spectra were recorded at 40 and 60 kHz MAS at sample temperatures of 293 and 291 K, respectively, using a conventional z-exchange scheme with a mixing time of 10 ms. For water suppression, 1–1 hard pulses were applied just before detection⁵². Both pulses were adjusted to 90°, separated by a delay of 45 μs corresponding to $1/4\nu_{\max}$ (with ν_{\max} being the difference in frequency of the protons of interest and the water protons).

In all other NMR experiments, cross polarization for heteronuclear magnetization transfers and MISSISSIPPI solvent suppression (except in ¹H–¹H exchange experiments) was used. (H)NH, (H)CANH, (H)CA(CO)NH, (H)CONH, (H)CO(CA)NH, (H)CBCANH, and (H)CBCA(CO)NH spectra were recorded with pulse sequences according to Barbet-Massin et al.²⁸, and experimental parameters as used in Nieuwkoop et al.⁵³. Tangential shapes were applied for heteronuclear cross polarization transfers. The ¹H–¹⁵N and ¹H–¹³C cross polarization steps were optimized around $w_1^H = 3\omega_R/2$ and $w_1^X = 1\omega_R/2$. The ¹³C–¹⁵N specific cross polarization transfers were optimized between $w_1^C = 3\omega_R/4$ and $w_1^N = 5\omega_R/4$, and $w_1^N = 1\omega_R/4$. For homonuclear (¹³C–¹³C) transfers, DREAM and INEPT was used

at 40 kHz and 60 kHz MAS, respectively. WALTZ-16 was applied for ^1H , ^{13}C , and ^{15}N decoupling during indirect evolution periods.

The ^1H - ^{13}C correlation spectra were recorded at 40 kHz (293 K sample temperature) and 60 kHz (291 K sample temperature) MAS either with ^{13}C -detection using one cross polarization transfer or with the proton-detected (H)CH pulse sequence employing two cross polarization steps. The latter was acquired again with MISSISSIPPI solvent suppression. For both ^1H - ^{13}C cross polarization and ^{13}C - ^1H cross polarization, the applied amplitudes were optimized around $w_1^{\text{H}} = 3\omega_{\text{R}}/2$ and $w_1^{\text{X}} = 1\omega_{\text{R}}/2$.

All spectra have been processed with Bruker Topspin Versions 3.4 or 4.0 and analyzed with CcpNmr Analysis Version 2.4. Gaussian (typically with a maximum at 0.04 and 40 Hz line broadening, except for the variable temperature series spectra for which a maximum at 0.1 and 100 Hz line broadening was used) and sine squared (sine bell shift of 2) apodization functions have been applied in the direct and indirect dimensions, respectively. For all spectra, baseline correction with a polynomial of degree 5 was used.

Ab initio molecular dynamics simulations. In order to quantify the excess proton localization in the vicinity of a carboxyl group, ab initio molecular dynamics simulations were performed in a model system, using a TZV2P basis set, the BLYP exchange-correlation functional and D3 dispersion correction in the CP2K 2.4 environment^{54–57}. The model system consists of a pair of deprotonated carboxyl groups, as commonly assumed in BR at D212 and D85, with a water molecule and one excess proton in between as shown in Fig. 3b. Note that this model agrees well with the BR crystal structure shown in Fig. 1b, which resolved a water molecule located right in between the D85 and D212 side chains. The simulation box size was optimized to be $15 \times 8 \times 8 \text{ \AA}^3$. The molecules were kept near the central axis of the simulation box by constraining the carbon atoms in y and z direction using Lagrangian multipliers implemented in the Shake algorithm. In addition, the water oxygen atom is constrained by a quadratic potential of 50 meV/\AA^2 in y and z direction to keep it close to the central axis. No constraints are applied along the axis connecting the two carbon atoms. A 40 ps molecular dynamics simulation was performed under NVT conditions at 300 K by coupling all atoms to a Nosé-Hoover chain of size three and decay time constant of 100 fs⁵⁸. The first 5 ps were dismissed for equilibration. Consequently, nine independent molecular dynamics simulations (5 ps each) were performed under NVE conditions starting from statistically independent snapshots of the NVT data. Proton distributions are computed from both, NVT and NVE simulations, thus from a total simulation time of 80 ps.

Reporting summary. Further information on research design is available in the Nature Research Reporting Summary linked to this article.

Data availability

The datasets generated during and/or analyzed during the current study are available from the corresponding author on reasonable request. The obtained NMR chemical shifts are deposited in the Biological Magnetic Resonance Bank database (accession number 50085).

Received: 11 July 2019; Accepted: 2 December 2019;

Published online: 03 January 2020

References

- Karplus, M. & Kuriyan, J. Molecular dynamics and protein function. *Proc. Natl Acad. Sci. USA* **102**, 6679–6685 (2005).
- Nango, E. et al. A three-dimensional movie of structural changes in bacteriorhodopsin. *Science* **354**, 1552–1557 (2016).
- Nogly, P. et al. Retinal isomerization in bacteriorhodopsin captured by a femtosecond x-ray laser. *Science* **361**, eaat0094 (2018).
- Gerwert, K., Freier, E. & Wolf, S. The role of protein-bound water molecules in microbial rhodopsins. *Biochim. Biophys. Acta* **1837**, 606–613 (2014).
- Luecke, H., Schobert, B., Richter, H. T., Cartailler, J. P. & Lanyi, J. K. Structure of bacteriorhodopsin at 1.55 Å resolution. *J. Mol. Biol.* **291**, 899–911 (1999).
- Henderson, R. et al. Model for the structure of bacteriorhodopsin based on high-resolution electron cryomicroscopy. *J. Mol. Biol.* **213**, 899–929 (1990).
- Henderson, R. & Unwin, P. N. T. 3-dimensional model of purple membrane obtained by electron-microscopy. *Nature* **257**, 28–32 (1975).
- Lozier, R. H., Bogomolni, R. A. & Stoerkenius, W. Bacteriorhodopsin: a light-driven proton pump in Halobacterium Halobium. *Biophys. J.* **15**, 955–962 (1975).
- Subramaniam, S. & Henderson, R. Molecular mechanism of vectorial proton translocation by bacteriorhodopsin. *Nature* **406**, 653–657 (2000).
- Mak-Jurkauskas, M. L. et al. Energy transformations early in the bacteriorhodopsin photocycle revealed by DNP-enhanced solid-state NMR. *Proc. Natl Acad. Sci. USA* **105**, 883–888 (2008).
- Wickstrand, C., Dods, R., Royant, A. & Neutze, R. Bacteriorhodopsin: would the real structural intermediates please stand up? *Biochim. Biophys. Acta* **1850**, 536–553 (2015).
- Neutze, R. et al. Bacteriorhodopsin: a high-resolution structural view of vectorial proton transport. *Biochim. Biophys. Acta* **1565**, 144–167 (2002).
- Shim, S., Dasgupta, J. & Mathies, R. A. Femtosecond time-resolved stimulated raman reveals the birth of bacteriorhodopsin's J and K intermediates. *J. Am. Chem. Soc.* **131**, 7592–7597 (2009).
- Lanyi, J. K. & Schobert, B. Structural changes in the L photointermediate of bacteriorhodopsin. *J. Mol. Biol.* **365**, 1379–1392 (2007).
- Bashford, D. & Gerwert, K. Electrostatic calculations of the pKa values of ionizable groups in bacteriorhodopsin. *J. Mol. Biol.* **224**, 473–486 (1992).
- Garczarek, F., Brown, L. S., Lanyi, J. K. & Gerwert, K. Proton binding within a membrane protein by a protonated water cluster. *Proc. Natl Acad. Sci. USA* **102**, 3633–3638 (2005).
- Spasov, V. Z., Luecke, H., Gerwert, K. & Bashford, D. pKa calculations suggest storage of an excess proton in a hydrogen-bonded water network in bacteriorhodopsin. *J. Mol. Biol.* **312**, 203–219 (2001).
- Freier, E., Wolf, S. & Gerwert, K. Proton transfer via a transient linear water-molecule chain in a membrane protein. *Proc. Natl Acad. Sci. USA* **108**, 11435–11439 (2011).
- Hutson, M. S., Alexiev, U., Shilov, S. V., Wise, K. J. & Braiman, M. S. Evidence for a perturbation of arginine-82 in the bacteriorhodopsin photocycle from time-resolved infrared spectra. *Biochemistry* **39**, 13189–13200 (2000).
- Lanyi, J. K. Bacteriorhodopsin. *Annu. Rev. Physiol.* **66**, 665–688 (2004).
- Kandori, H. Role of internal water molecules in bacteriorhodopsin. *Biochim. Biophys. Acta* **1460**, 177–191 (2000).
- Zheng, L., Fishbein, K. W., Griffin, R. G. & Herzfeld, J. Two-dimensional solid-state proton NMR and proton exchange. *J. Am. Chem. Soc.* **115**, 6254–6261 (1993).
- Lanyi, J. K. Proton transfers in the bacteriorhodopsin photocycle. *Biochim. Biophys. Acta* **1757**, 1012–1018 (2006).
- Sass, H. J. et al. Structural alterations for proton translocation in the M state of wild-type bacteriorhodopsin. *Nature* **406**, 649–653 (2000).
- Royant, A. et al. Helix deformation is coupled to vectorial proton transport in the photocycle of bacteriorhodopsin. *Nature* **406**, 645–648 (2000).
- Zhou, D. H. et al. Proton-detected solid-state NMR spectroscopy of fully protonated proteins at 40 kHz magic-angle spinning. *J. Am. Chem. Soc.* **129**, 11791–11801 (2007).
- Chevelkov, V. et al. ^1H detection in MAS solid-state NMR spectroscopy of biomacromolecules employing pulsed field gradients for residual solvent suppression. *J. Am. Chem. Soc.* **125**, 7788–7789 (2003).
- Barbet-Massin, E. et al. Rapid proton-detected NMR assignment for proteins with fast magic angle spinning. *J. Am. Chem. Soc.* **136**, 12489–12497 (2014).
- Lalli, D. et al. Proton-based structural analysis of a heptahelical transmembrane protein in lipid bilayers. *J. Am. Chem. Soc.* **139**, 13006–13012 (2017).
- Dannatt, H. R. W. et al. ^{13}C - and ^1H -detection under fast MAS for the study of poorly available proteins: application to sub-milligram quantities of a 7 trans-membrane protein. *J. Biomol. NMR* **62**, 17–23 (2015).
- Higman, V. A. et al. The conformation of bacteriorhodopsin loops in purple membranes resolved by solid-state MAS NMR spectroscopy. *Angew. Chem. Int. Ed.* **50**, 8432–8435 (2011).
- Mogi, T., Stern, L. J., Marti, T., Chao, B. H. & Khorana, H. G. Aspartic acid substitutions affect proton translocation by bacteriorhodopsin. *Proc. Natl Acad. Sci. USA* **85**, 4148–4152 (1988).
- Mei, G. et al. Raman spectroscopy of a near infrared absorbing proteorhodopsin: similarities to the bacteriorhodopsin O photointermediate. *PLoS One* **13**, e0209506 (2018).
- Tittor, J. et al. Chloride and proton transport in bacteriorhodopsin mutant D85T: different modes of ion translocation in a retinal protein. *J. Mol. Biol.* **271**, 405–416 (1997).
- Miercke, L. J. W. et al. Wild-type and mutant bacteriorhodopsins D85N, D96N, and R82Q: purification to homogeneity, pH dependence of pumping and electron diffraction. *Biochemistry* **30**, 3088–3098 (1991).
- Brown, L. S., Bonet, L., Needleman, R. & Lanyi, J. K. Estimated acid dissociation constants of the Schiff base, Asp-85, and Arg-82 during the bacteriorhodopsin photocycle. *Biophys. J.* **65**, 124–130 (1993).
- Metz, G., Siebert, F. & Engelhard, M. Asp⁸⁵ is the only internal aspartic acid that gets protonated in the M intermediate and the purple-to-blue transition of bacteriorhodopsin. *FEBS Lett.* **303**, 237–241 (1992).
- Mäemets, V. & Koppel, I. ^{17}O and ^1H chemical shifts of hydroxide and hydronium ion in aqueous solutions of strong electrolytes. *J. Chem. Soc. Faraday Trans.* **93**, 1539–1542 (1997).

39. Ni, Q. Z. et al. Primary transfer step in the light-driven ion pump bacteriorhodopsin: an irreversible U-turn revealed by dynamic nuclear polarization-enhanced magic angle spinning NMR. *J. Am. Chem. Soc.* **140**, 4085–4091 (2018).
40. Oesterhelt, D., Meentzen, M. & Schuhmann, L. Reversible dissociation of the purple complex in bacteriorhodopsin and identification of 13-*cis* and all-*trans*-retinal as its chromophors. *Eur. J. Biochem.* **40**, 453–463 (1973).
41. Bondar, A.-N., Smith, J. C. & Elstner, M. Mechanism of a proton pump analyzed with computer simulations. *Theor. Chem. Acc.* **125**, 353–363 (2010).
42. Druckmann, S., Ottolenghi, M., Pande, A., Pande, J. & Callender, R. H. Acid-base equilibrium of the Schiff base in bacteriorhodopsin. *Biochemistry* **21**, 4953–4959 (1982).
43. Eisenstein, L. et al. FTIR difference studies on apoproteins. Protonation states of aspartic and glutamic acid residues during the photocycle of bacteriorhodopsin. *J. Am. Chem. Soc.* **109**, 6860–6862 (1987).
44. Rothschild, K. J., Zagaeski, M. & Cantore, W. A. Conformational changes of bacteriorhodopsin detected by Fourier transform infrared difference spectroscopy. *Biochem. Biophys. Res. Commun.* **103**, 483–489 (1981).
45. Marx, D., Tuckerman, M. E., Hutter, J. & Parrinello, M. The nature of the hydrated excess proton in water. *Nature* **397**, 601–604 (1999).
46. Rozas, I., Alkorta, I. & Elguero, J. Bifurcated hydrogen bonds: three-centered interactions. *J. Phys. Chem. A* **102**, 9925–9932 (1998).
47. Eckert, M. & Zundel, G. Energy surfaces and proton polarizability of hydrogen-bonded chains: an ab initio treatment with respect to the charge conduction in biological systems. *J. Phys. Chem.* **92**, 7016–7023 (1988).
48. Kandt, C., Schlitter, J. & Gerwert, K. Dynamics of water molecules in the bacteriorhodopsin trimer in explicit lipid/water environment. *Biophys. J.* **86**, 705–717 (2004).
49. Shibata, M., Tanimoto, T. & Kandori, H. Water molecules in the Schiff base region of bacteriorhodopsin. *J. Am. Chem. Soc.* **125**, 13312–13313 (2003).
50. Vogt, A. et al. Conversion of a light-driven proton pump into a light-gated ion channel. *Sci. Rep.* **5**, 16450 (2015).
51. Zhou, D. H. & Rienstra, C. M. High-performance solvent suppression for proton detected solid-state NMR. *J. Magn. Reson.* **192**, 167–172 (2008).
52. Clore, G. M., Kimber, B. J. & Gronenborn, A. M. The 1-1 hard pulse: a simple and effective method of water resonance suppression in FT ¹H NMR. *J. Magn. Reson.* **54**, 170–173 (1983).
53. Nieuwkoop, A. J. et al. Sensitivity and resolution of proton detected spectra of a deuterated protein at 40 and 60 kHz magic-angle-spinning. *J. Biomol. NMR* **61**, 161–171 (2015).
54. Becke, A. D. Density-functional exchange-energy approximation with correct asymptotic behavior. *Phys. Rev. A* **38**, 3098–3100 (1988).
55. VandeVondele, J. & Hutter, J. Gaussian basis sets for accurate calculations on molecular systems in gas and condensed phases. *J. Chem. Phys.* **127**, 114105 (2007).
56. Hutter, J., Iannuzzi, M., Schiffmann, F. & VandeVondele, J. Cp2k: atomistic simulations of condensed matter systems. *Wiley Interdiscip. Rev. Comput. Mol. Sci.* **4**, 15–25 (2014).
57. Grimme, S., Antony, J., Ehrlich, S. & Krieg, H. A consistent and accurate ab initio parametrization of density functional dispersion correction (DFT-D) for the 94 elements H-Pu. *J. Chem. Phys.* **132**, 154104 (2010).
58. Nosé, S. A unified formulation of the constant temperature molecular dynamics methods. *J. Chem. Phys.* **81**, 511–519 (1984).

Acknowledgements

We thank Margrit Michalsky and Thi Bich Thao Nguyen for excellent technical assistance and production of purple membranes, and Janos Lanyi, Dieter Oesterhelt and Markus Lange, Actilor GmbH, for the *Halobacterium salinarum* strains BR-R82Q, BR-D85T, and BR-D96N. Initial efforts in experimental design by Marcella Orwick-Rydmark and support in NMR data analysis by Lisa Gerland is kindly acknowledged. This study received funding by the Deutsche Forschungsgemeinschaft through SFB 1078 to Roland R. Netz (C1), Peter Hegemann (B1, B2), and Hartmut Oschkinat (B1). Daniel Friedrich received support by the Human Frontier Science Program (HFSP, LT000022/2019-L) and is a non-stipendiary Fellow of the European Molecular Biology Organization (EMBO, ALTF 35-2019).

Author contributions

D.F., P.H., and H.O. designed the study. D.F. and A.J.N. designed and performed NMR experiments. F.N.B. and R.R.N. designed, performed and analyzed ab initio molecular dynamics simulations. D.F. and H.O. analyzed and interpreted data. D.F., P.H., and H.O. wrote the paper with contributions from all authors.

Competing interests

The authors declare no competing interests.

Additional information

Supplementary information is available for this paper at <https://doi.org/10.1038/s42003-019-0733-7>.

Correspondence and requests for materials should be addressed to H.O.

Reprints and permission information is available at <http://www.nature.com/reprints>

Publisher's note Springer Nature remains neutral with regard to jurisdictional claims in published maps and institutional affiliations.



Open Access This article is licensed under a Creative Commons Attribution 4.0 International License, which permits use, sharing, adaptation, distribution and reproduction in any medium or format, as long as you give appropriate credit to the original author(s) and the source, provide a link to the Creative Commons license, and indicate if changes were made. The images or other third party material in this article are included in the article's Creative Commons license, unless indicated otherwise in a credit line to the material. If material is not included in the article's Creative Commons license and your intended use is not permitted by statutory regulation or exceeds the permitted use, you will need to obtain permission directly from the copyright holder. To view a copy of this license, visit <http://creativecommons.org/licenses/by/4.0/>.

© The Author(s) 2020